



Published in final edited form as:

Inorg Chem. 2020 November 16; 59(22): 16319–16327. doi:10.1021/acs.inorgchem.0c02115.

A C^N Cycloplatinated(II) Fluoride Complex: Photophysical Studies and Csp³–F Bond Formation

Jiyun Hu,

Department of Chemistry and Biochemistry, University of Arkansas, Fayetteville, Arkansas, 72701, United States

Mahshid Nikravesh,

Department of Chemistry, Institute for Advanced Studies in Basic Sciences (IASBS), Zanjan, 45137-66731, Iran

Hamid R. Shahsavari,

Department of Chemistry, Institute for Advanced Studies in Basic Sciences (IASBS), Zanjan, 45137-66731, Iran; Department of Chemistry and Biochemistry, University of Arkansas, Fayetteville, Arkansas, 72701, United States

Reza Babadi Aghakhanpour,

Department of Chemistry, Institute for Advanced Studies in Basic Sciences (IASBS), Zanjan, 45137-66731, Iran

Arnold L. Rheingold,

Department of Chemistry, University of California, San Diego, La Jolla, California 92093, United States

Mia Alshami,

Department of Chemistry and Biochemistry, University of Arkansas, Fayetteville, Arkansas, 72701, United States

Yoshie Sakamaki,

Department of Chemistry and Biochemistry, University of Arkansas, Fayetteville, Arkansas, 72701, United States

Hudson Beyzavi

Corresponding Author: Hamid R. Shahsavari – shahsavari@iasbs.ac.ir. Hudson Beyzavi – beyzavi@uark.edu.

Present Addresses

H.R.S on sabbatical leave from IASBS, Zanjan, Iran.

Author Contributions

J. Hu and M. Nikravesh contributed equally to this work.

Supporting Information.

NMR and HR ESI-MS spectra of **2**, excitation and emission spectra, computational data of complexes (PDF). Crystallographic data (CIF). Cartesian coordinates (XYZ).

Accession Codes

CCDC 2008721 contains the supplementary crystallographic data for this paper. These data can be obtained free of charge *via* www.ccdc.cam.ac.uk/data_request/cif, or by emailing data_request@ccdc.cam.ac.uk, or by contacting The Cambridge Crystallographic Data Centre, 12 Union Road, Cambridge CB2 1EZ, UK; fax: +44 1223 336033.

The authors declare no competing financial interest.

Department of Chemistry and Biochemistry, University of Arkansas, Fayetteville, Arkansas, 72701, United States

Abstract

This work reports the synthesis and characterization of a new C^N-based cycloplatinated(II) fluoride complex [Pt(ppy)(PPh₃)F] (**2**, ppy = 2-phenylpyridinate), involving a Pt–F bond. The new complex is highly luminescent in green area with a high quantum yield of 94.6% at 77K. A comparison study of the heavier of halogen derivatives reveals a descending emission quantum yield order of F > Cl > Br > I. Time-dependent density functional theory (TD-DFT) calculations ascribe the decreased emission efficiency to the decreasing trend of intra ligand (IL) transition from F to I, which accounts for the major radiative pathway. In addition, **2** is capable of the fluorinating alkyl halides leading to Csp³–F bond formation at room temperature.

Introduction

Halide ions are among the most common ligands used for stabilizing transition metals. The size, σ -bond donation ability, *trans* effect, and bond strengths to low oxidation state metals increase down the halide group, while the π -bond donation and bond strength to high oxidation state metals decrease from F to I.¹ As a result, transition metal complexes usually show interesting halide effect in reactivity and properties such as luminescence. While transition metal complexes with Cl, Br, and I ligands are very common, the F containing analogues are much less available, especially for late transition metals cations in low oxidation states,^{2–5} thus preventing a complete study across the group. For example, halide ligands (Cl, Br, I) have been shown to largely influence the emission properties of Pt(II)^{6–9}, Pt(IV)^{10, 11}, and Cu(I)^{12–15} complexes. The scarcity of transition metal fluoride complexes is largely due to their high reactivity and the limited synthetic methods, as predicted by the hard/soft acid–base theory that the fluoride ion (hard base) is mismatched with soft acid such as Pt(II), Pd(II), Au(I).¹⁶

Our groups have been actively studying cycloplatinated complexes due to their intriguing photophysical and biological properties.^{17–22} Some Pt(II)^{23–28} and Pt(IV)^{29–37} fluoride complexes are known in literature, however, cycloplatinated complexes bearing a Pt–F bond are unprecedented.^{38–40} To the best of our knowledge, only one report discussed the halide effect on the photophysical properties of Pt(IV) complexes involving all the F, Cl, Br, and I ligands.¹⁰ A systematic investigation of the halide effect on the photophysical properties of Pt(II) is not available. Herein, we report the synthesis, photophysical properties and reactivity of a C^N-based cycloplatinated(II) complex with a fluoride ligand.

Results and Discussion

Synthesis and Structural Characterization

The Pt fluoride complex [Pt(ppy)(PPh₃)F] (**2**, ppy = 2-phenylpyridinate) was efficiently synthesized through F/X exchange from its heavier halogen counterparts [Pt(ppy)(PPh₃)X] (**1**, X = Cl, **1a**; Br, **1b**; I, **1c**)^{41, 42} using AgF as the fluoride source (Scheme 1, yield > 85%).

The halide metathesis reaction was performed in CH_2Cl_2 at room temperature with 1.4 equiv. of AgF (see the Experimental Section for details).

The successful formation of **2** with Pt–F bond was first identified using the multinuclear 1D (Figures 1 and S1–S5) and 2D (Figures S6–S8) NMR spectroscopy. The ^{19}F NMR spectrum of **2** shows a sharp doublet signal ($^2J_{\text{PF}} = 17$ Hz) flanked by Pt satellites ($^1J_{\text{PtF}} = 340$ Hz) at $\delta = -241.4$ ppm providing direct evidence of Pt–F bonding. Correspondingly, a doublet signal appears in the $^{31}\text{P}\{^1\text{H}\}$ NMR spectrum of **2** ($\delta = 24.0$ ppm) which has a $^2J_{\text{PF}}$ coupling constant of 17 Hz consistent with that observed from ^{19}F NMR spectroscopy (Figure 1). This doublet signal has Pt satellites with $^1J_{\text{PtP}} = 4406$ Hz which is normal for direct Pt–P bonds in Pt(II) complexes.^{17, 21, 42} Expectedly, the corresponding $^{195}\text{Pt}\{^1\text{H}\}$ NMR spectrum includes a sharp doublet of doublet signal at $\delta = -3917$ ppm ($^1J_{\text{PtP}} = 4411$ Hz, $^1J_{\text{PtF}} = 342$ Hz) due to the coupling with both the coordinated P and F atoms, respectively.

The HR-ESI-Mass spectrum of **2** (Figure S9) shows an ion with an isotope pattern diagnostic for $[\text{M}-\text{F}]^+$ moiety ($m/z = 611.1206$). Finally, the molecular structure of **2** was unambiguously characterized by single crystal X-ray crystallography (Figure 2). The crystallographic data (Table S1) and the selected bond lengths and angles are collected in Table S2. The crystal structure of **2** clearly indicates that the fluoride ligand is directly bound to the Pt center and located *trans* to the ligating C atom of the ppy ligand. The bond length of Pt–F is 2.042 Å, in the typical range of tetracoordinated platinum fluoride complexes.^{23–28} The platinum adopts a distorted-square-planar coordination geometry with angles ranging from 81.38 to 98.88° and the maximum deviation from the mean plane through PtCNPF is 0.018 Å. The fluoride ligand involves hydrogen bonding interactions with co-crystallized CH_2Cl_2 solvent⁴³ (1.950 Å, Figure 2), H^6 of ppy ligand⁴² (2.306 Å), and one hydrogen from PPh_3 (2.209 Å) of the vicinal molecule. These interactions are much shorter than the sum of the van der Waals radii of H and F (2.68 Å)^{44–47} (Figure S10).

Photophysical Properties

The fluoride complex **2** is highly emissive in green area in different states and temperature conditions. In solid state at 298 K, **2** gives a completely structured emission band centered at 490 nm with a vibronic progression at 523 nm and a shoulder at around 560 nm, indicating a large composition of ^3IL with small contribution of $^3\text{MLCT}$ in the emissive state (Figure 3). The lifetime of **2** was measured to be 11.6 μs , confirming the phosphorescence character of the emission. By lowering the temperature down to 77 K, **2** exhibits a much brighter emission with a significant increase in quantum yield (Φ) from 53.1 to 94.6%. There is no tangible change in the position and shape of the emission band at 77 K compared to that of at room temperature (Figure 3). In CH_2Cl_2 solution state at 298 K, **2** keeps its emission in green region ($\Phi = 8.4\%$), yielding a structured emission band with a slight blue shift compared with that of the solid state (Figure 3). The emission band of the frozen solution (77 K) appears at 480 nm with a slight blue shift and more structured shape compared with that of at 298 K (Figure 3).

Interestingly, in solid state the similar emission bands but with decreased intensities were observed from **2** to **1c** (F to I), while **1c** is practically non-emissive (Figure 4 and Table 1).

The descending trend of Φ values for **2** (53.1%), **1a** (47.0%) and **1b** (31.0%) certifies this observation. This was supported by the obtained non-radiative rate constants (k_{nr}) of the complexes (**2** [4.06×10^4], **1a** [7.36×10^4] and **1b** [10.0×10^4]) which are on the increase from **2** to **1b**.

To investigate the nature of electronic transitions, the UV-vis spectra were obtained for **2** and **1a–c** in CH_2Cl_2 (Figures 5 and S11, Table S3). Density functional theory (DFT) and time-dependent DFT (TD-DFT) calculation methods were carried out for better understanding of the ground and excited states. All complexes were optimized in CH_2Cl_2 solution and gas phase (considered as solid state). Besides, their DFT-optimized structures (Figure S12) and the selected geometrical parameters (Table S4) are given in the Supporting Information. Then, the frontier molecular orbitals (MOs) involving “HOMO to HOMO-5” and “LUMO to LUMO+5” were calculated for all the complexes (Tables S5–S8 and visual plots in Figures S13–S16). In all the cases, HOMO is mostly localized on the Pt, ppy and halogen moieties, of which the contribution of halogen ligand increases from F to I. However, LUMO is remarkably centered on the ppy ligand (around 88%). The contribution of PPh_3 is negligible in HOMO and LUMO levels, but it considerably increases in lower HOMOs and higher LUMOs.

TD-DFT calculated electronic transitions are in good agreement with the experimental UV-vis absorption spectra for all the complexes (Figure 5). The low energy region 350–425 nm is related to the $S_0 \rightarrow S_1$ transition which is mainly contributed by the HOMO \rightarrow LUMO transition (> 90%). This region is assigned as the mixed $^1\text{IL}/^1\text{MLCT}$ and $^1\text{XLCT}$ (L = ppy, X = halides) characters. In compliance with the experimental data, the low energy band in **2** is red shifted compared to those of the other derivatives (Figure S17). For the more intense absorbing high energy bands (250–350 nm), in addition to IL, MLCT, and XLCT, some other characters like $\text{ML}'\text{CT}$, $\text{LL}'\text{CT}$, $\text{L}'\text{LCT}$ and $\text{XL}'\text{CT}$ ($\text{L}' = \text{PPh}_3$) can be observed, indicating the important role of PPh_3 as the beginning or destination of the electronic transitions (Tables S9–S12).

The theoretical emission wavelengths were calculated for **2**, **1a** and **1b**, using the energy gap between the optimized structures of S_0 and T_1 states in the gas phase. The calculated energy gaps between S_0 and T_1 are 2.516 (**2**), 2.595 (**1a**) and 2.579 (**1b**) eV, corresponding to the emission wavelengths of 493, 478, and 481 nm, respectively. These theoretical emissions are very close to the corresponding experimental values at 298 K (Table 1). To obtain further insight into the nature of the emissions, the frontier molecular orbitals were calculated for S_0 (HOMO and LUMO) and T_1 (LSOMO and HSOMO) states in the gas phase. Figure 6 depicts the HOMO-LUMO and LSOMO-HSOMO energy levels diagram for **2** while those of **1a** and **1b** are shown in Figures S18 and S19, respectively, and summarized in Table 2. For **2**, LSOMO is close to HOMO in terms of the composition and energy. HSOMO also resembles LUMO (both localized on ppy moiety), but with a significant stabilization in energy. By looking at the LSOMO and HSOMO plots, the mixed $^3\text{IL}/^3\text{MLCT}/^3\text{XLCT}$ emission character can be concluded for the complexes.

In order to understand the halide effect on the emission of these Pt complexes, TD-DFT calculations were performed in the gas phase. Figure 7 demonstrates the comparative

diagram for the energy levels of the calculated MOs of **1a–c** and **2**. Similar to the solution states, the lowest electronic transitions are attributed to the HOMO→LUMO transition for all the complexes wherein the HOMO-LUMO energy gap is almost on the decrease from F to I (**2** [3.826 eV], **1a** [3.828 eV], **1b** [3.718 eV] and **1c** [3.512 eV]). In all the cases, based on the contribution percentages shown in Table 2, the HOMO→LUMO transition is assigned as mixed IL/MLCT/XLCT characters. The contribution of halide ligands in HOMO increases from F to I (Table 2, **2** [11 %], **1a** [30 %], **1b** [45 %] and **1c** [62 %]), while the contribution of ppy ligand decreases (Table 2, **2** [35 %], **1a** [27 %], **1b** [18 %] and **1c** [10 %]). As a result, the XLCT character grows and the IL character concedes (intra ligand transition in ppy) from F to I. Additionally, as can be observed in Figure 7, the energies of the d_{σ}^* orbitals of **2** are higher than those of the other complexes **1a–c**. It suggests the higher energies of the MC states for **2** which qualitatively explain the trend of emission strength for all the complexes.

C_{sp^3} -F Bond Formation

Transition metal fluoride complexes are important intermediates in C–F bond activation/formation reactions.^{38, 48–52} To test its reactivity for fluorination reaction, **2** was reacted with methyl iodide, ethyl iodide and allyl bromide. In situ ¹⁹F NMR monitoring of the reactions (Figures 8, S20 and S21) showed the consumption of **2** and the concomitant formation of CH₃–F, C₂H₅–F, and allyl fluoride respectively at room temperature. The formation of the corresponding Pt complexes **1b** and **1c**, were observed in their ¹H and ³¹P{¹H} NMR spectra.⁴² The reaction was much faster for allyl bromide (completed in 10 min at room temperature) compared with that for methyl iodide and ethyl iodide. The higher reactivity of allyl bromide might result from its more electron-deficient allylic carbon and/or its strong interaction with the metal center *via* coordination.⁵³

Conclusions

In summary, we report here the first example of a C^N-type cycloplatinated(II) fluoride complex. The complex exhibits an emission centered on the cyclometalated ligand in green region, being stronger (solid and solution) than its heavier halide derivatives (F[>] Cl[>] Br[>] I). The theoretical calculations indicated that the nature of halogen ligand significantly affects the emissions. TD-DFT calculations exhibited that, from F to I, the contribution of XLCT character in HOMO→LUMO transition is intensified, lowering the contribution of IL character as the center of emission. Besides, the new Pt–F complex is able to participate in C_{sp^3} -F bond formation reactions with alkyl halides. We are currently investigating the ligand electronic effect on the reactivity, the scope of the substrates and the mechanism of C–F bond formation.

Experimental Section

General Remarks

¹H (700 MHz), ¹³C{¹H} (176 MHz), ¹⁹F (376 MHz), ³¹P{¹H} (162 MHz) and ¹⁹⁵Pt{¹H} (64 MHz) NMR spectra were recorded on Bruker Avance 700, 400 or 300 MHz instruments at room temperature. All chemical shifts (δ) are reported in ppm relative to their

corresponding external standards (SiMe₄ for ¹H and ¹³C{¹H}, CFC₃ for ¹⁹F, 85% H₃PO₄ for ³¹P{¹H}, Na₂PtCl₆ for ¹⁹⁵Pt{¹H}). The instrument for HR ESI-Mass measurement was a Shimadzu IT-TOF with an electrospray ionization source, which is part of the Arkansas Statewide Mass Spectrometry Facility. UV-vis absorption spectra were recorded on a JASCO V-770 UV-visible/NIR spectrophotometer. Emission spectra were measured on a JASCO FP-8500 spectrofluorometer. The lifetimes were measured in the phosphorimeter mode and the quantum yields of the complexes were measured using an integrating sphere. The 2-phenylpyridine (ppy), triphenylphosphine (PPh₃), silver fluoride (AgF) and all the other chemicals were purchased from commercial resources. All the reactions were carried out under Argon atmosphere and in the common solvents and all solvents were purified and dried according to standard procedures before using.⁵⁴ The complexes [Pt(ppy)(PPh₃)Cl], **1a**, [Pt(ppy)(PPh₃)Br], **1b**, [Pt(ppy)(PPh₃)I], **1c**, were prepared as published methods.⁴² The NMR labeling is shown in Scheme 1 for clarifying the chemical shift assignments.

Synthesis of [Pt(ppy)(PPh₃)F], **2**

To a solution of **1a** (200 mg, 0.31 mmol, 1 eq.) in CH₂Cl₂ (20 mL) was added AgF (55 mg, 0.43 mmol, 1.4 eq.). The reaction mixture was stirred for 3 days in dark at room temperature, and then filtered through cotton/Celite in a glass Pasteur pipette to remove AgCl. The resulting greenish solution was concentrated to a small volume (~ 1 mL) and *n*-hexane (5 mL) was added to precipitate **2** as a green solid. Yield: 87% (169 mg, 0.27 mmol). HR ESI-MS(+) *m/z* Calcd. for C₂₉H₂₃NPPt [M-F]⁺ 611.1215; Found 611.1206. Elem. Anal. Calcd for C₂₉H₂₃FNPt (630.55): C, 55.24; H, 3.68; N, 2.22; Found: C, 55.41; H, 3.74; N, 2.19. ¹H NMR (700 MHz, CD₂Cl₂, 295 K): δ 9.07 (ddd, ³J_{PtH} = 28.3 Hz, ³J_{HH} = 4.8 Hz, ⁴J_{FH} = 8.7 Hz, ⁴J_{PH} = 4.1 Hz, 1H, H⁶), 7.94 (t, ³J_{HH} = 7.9 Hz, 1H, H⁴), 7.81 (d, ³J_{HH} = 7.9 Hz, 1H, H³), 7.74 (dd, ³J_{HH} = 7.8 Hz, ³J_{PH} = 11.2 Hz, 6H, H^o of PPh₃), 7.51 (d, ³J_{HH} = 7.6 Hz, 1H, H¹²), 7.48 (t, ³J_{HH} = 7.2 Hz, 3H, H^p of PPh₃), 7.41 (t, ³J_{HH} = 7.2 Hz, 6H, H^m of PPh₃), 7.36 (t, ³J_{HH} = 6.3 Hz, 1H, H⁵), 6.93 (t, ³J_{HH} = 7.4 Hz, 1H, H¹¹), 6.52 (ddd, ³J_{PtH} = 49.1 Hz, ³J_{HH} = 7.6 Hz, ⁴J_{PH} = 3.9 Hz, 1H, H⁹), 6.50 (t, ³J_{HH} = 7.3 Hz, 1H, H¹⁰); ¹³C{¹H} NMR (376 MHz, CD₂Cl₂, 295 K): δ 164.9 (d, ³J_{Pc} = 3 Hz, C²), 146.8 (d, ²J_{Pc} = 21 Hz, ³J_{Fc} = 13 Hz, C⁶), 146.1 (s, C⁷), 140.6 (s, C⁴), 139.6 (dd, ²J_{Pc} = 83 Hz, ³J_{Fc} = 7 Hz, ³J_{Pc} = 5 Hz, C⁹), 135.6 (d, ³J_{Pc} = 38 Hz, ²J_{Pc} = 13 Hz, C^o of PPh₃), 131.3 (d, ⁴J_{Pc} = 2 Hz, C^p of PPh₃), 129.8 (dd, ³J_{Pc} = 57 Hz, ⁴J_{Pc} = 2 Hz, ⁴J_{Fc} = 4 Hz, C¹⁰), 129.7 (d, ¹J_{Pc} = 61 Hz, C^{ipso} of PPh₃), 128.6 (d, ³J_{Pc} = 10 Hz, C^m of PPh₃), 124.0 (s, ³J_{Pc} = 30 Hz, C¹²), 123.4 (s, C¹¹), 122.3 (d, ³J_{Pc} = 16 Hz, ⁴J_{Pc} = 2 Hz, C⁵), 118.7 (d, ³J_{Pc} = 17 Hz, ⁴J_{Pc} = 2 Hz, C³); ¹⁹F NMR (376 MHz, CD₂Cl₂, 295 K): δ -241.4 (d, ¹J_{PtF} = 340 Hz, ²J_{PF} = 17 Hz, 1F); ³¹P{¹H} NMR (162 MHz, CD₂Cl₂, 295 K): δ 24.0 (d, ¹J_{PtP} = 4406 Hz, ²J_{PF} = 17 Hz, 1P); ¹⁹⁵Pt{¹H} NMR (64 MHz, CD₂Cl₂, 295 K): δ -3917 (dd, ¹J_{PtP} = 4411 Hz, ¹J_{PtF} = 342 Hz, 1Pt).

Monitoring the Reaction of **2** with Alkyl Halides (MeI, EtI and AllylBr) by NMR Spectroscopy

To a solution of **2** (10 mg, 0.016 mmol) in acetone-*d*₆ (0.75 mL) in an NMR tube was added the appropriate alkyl halides (10 μL, 0.16 mmol for Me-I; 26 μL, 0.32 mmol for Et-I; 2 μL, 0.025 mmol for allyl bromide) at 298 K. The tube was then placed in the probe of the NMR spectrometer and NMR spectra were obtained at appropriate time intervals (Figures 8, S20 and S21).

X-ray Structure Determination

The appropriate crystals of **2** were obtained by slow evaporation of its saturated solution in CH₂Cl₂/diisopropyl ether at room temperature. Single crystal X-ray diffraction intensity data of **2** was collected at 100(2) K using a Bruker APEX-II CCD diffractometer equipped with graphite monochromated MoK α radiation ($\lambda = 0.71073 \text{ \AA}$). Data reduction was carried out using the program Bruker SAINT⁵⁵ and an empirical absorption correction was applied based on multi-scan method.⁵⁶ The structure of **2** was solved by direct method and refined by the full-matrix least-square technique on $|F|^2$ with anisotropic thermal parameters to describe the thermal motions of all non-hydrogen atoms using the programs (SHELXS-14)⁵⁷ and (SHELXL-18),⁵⁸ respectively. All hydrogen atoms were located from difference Fourier map and refined isotropically. The summary of crystal data and relevant structure refinement parameters for **2** (CCDC 2008721) are given in Table S1.

Computational Details

Density functional calculations were performed with the program suite Gaussian 09⁵⁹ using the B3LYP level of theory.^{60–62} The LANL2DZ basis set was chosen to describe Pt^{63, 64} and the 6–31G(d) basis set was chosen for other atoms. The geometries of complexes were fully optimized by employing the density functional theory without imposing any symmetry constraints. In order to ensure the optimized geometries, frequency calculations were performed employing analytical second derivatives. Time-dependent DFT (TD-DFT) calculations were carried out at the same level of theory and basis sets. Solvent effects have been considered by the conductor-like polarizable continuum model (CPCM)^{65, 66}. The calculations for the electronic absorption spectra by time-dependent DFT (TD-DFT) were performed at the same level of theory.

Supplementary Material

Refer to Web version on PubMed Central for supplementary material.

ACKNOWLEDGMENT

H.B. gratefully acknowledges the financial support through the startup funds from the University of Arkansas and the NIH-NIGMS (GM132906). The Institute for Advanced Studies in Basic Sciences (IASBS) Research Council (G2020IASBS32629) and the Iran National Science Foundation (Grant no. 97007977) are also gratefully acknowledged. H.R.S. wishes to acknowledge IASBS for their sabbatical leave at University of Arkansas.

References

1. Fagnou K; Lautens M, Halide Effects in Transition Metal Catalysis. *Angew. Chem. Int. Ed* 2002, 41, 26–47.
2. Doherty NM; Hoffmann NW, Transition-Metal Fluoro Compounds Containing Carbonyl, Phosphine, Arsine, and Stibine Ligands. *Chem. Rev* 1991, 91, 553–573.
3. Murphy EF; Murugavel R; Roesky HW, Organometallic Fluorides: Compounds Containing Carbon–Metal–Fluorine Fragments of d-Block Metals. *Chem. Rev* 1997, 97, 3425–3468. [PubMed: 11851496]
4. Nahra F; Brill M; Gómez-Herrera A; Cazin CS; Nolan SP, Transition Metal Bifluorides. *Coord. Chem. Rev* 2016, 307, 65–80.
5. Pagenkopf BL; Carreira EM, Transition Metal Fluoride Complexes in Asymmetric Catalysis. *Chem. Eur. J* 1999, 5, 3437–3442.

6. Irmiler P; Winter RF, Complexes trans-Pt (BODIPY)X(PEt₃)₂: Excitation Energy-dependent Fluorescence and Phosphorescence Emissions, Oxygen Sensing and Photocatalysis. *Dalton Trans.* 2016, 45, 10420–10434. [PubMed: 27255789]
7. Paziresh S; Aghakhanpour RB; Rashidi M; Nabavizadeh SM, Simple Tuning of the Luminescence Properties of the Double Rollover Cycloplatinated(II) Structure by Halide Ligands. *New J. Chem* 2018, 42, 1337–1346.
8. Sangari MS; Haghghi MG; Nabavizadeh SM; Pfitzner A; Rashidi M, Influence of Ancillary Ligands on the Photophysical Properties of Cyclometalated Organoplatinum(II) Complexes. *New J. Chem* 2018, 42, 8661–8671.
9. Lázaro A; Serra O; Rodríguez L; Crespo M; Font-Bardia M, Luminescence Studies of New [C,N,N'] Cyclometalated Platinum(II) and Platinum(IV) Compounds. *New J. Chem* 2019, 43, 1247–1256.
10. Juliá F; García-Legaz M-D; Bautista D; González-Herrero P, Influence of Ancillary Ligands and Isomerism on the Luminescence of Bis-cyclometalated Platinum(IV) Complexes. *Inorg. Chem* 2016, 55, 7647–7660. [PubMed: 27438708]
11. Lázaro A; Balcells C; Quirante J; Badia J; Baldomà L; Ward JS; Rissanen K; Font-Bardia M; Rodríguez L; Crespo M, Luminescent Pt^{II} and Pt^{IV} Platinacycles with Anticancer Activity Against Multiplatinum-Resistant Metastatic CRC and CRPC Cell Models. *Chem. Eur. J* 2020, 26, 1947–1952.
12. Zhang J; Duan C; Han C; Yang H; Wei Y; Xu H, Balanced Dual Emissions from Tridentate Phosphine-Coordinate Copper(I) Complexes toward Highly Efficient Yellow OLEDs. *Adv. Mater* 2016, 28, 5975–5979. [PubMed: 27167890]
13. Jia J-H; Chen X-L; Liao J-Z; Liang D; Yang M-X; Yu R; Lu C-Z, Highly Luminescent Copper(I) Halide Complexes Chelated with a Tetradentate Ligand (PNNP): Synthesis, Structure, Photophysical Properties and Theoretical Studies. *Dalton Trans* 2019, 48, 1418–1426. [PubMed: 30628618]
14. Baranov AY; Berezin AS; Samsonenko DG; Mazur AS; Tolstoy PM; Plyusnin VF; Kolesnikov IE; Artem'Ev AV, New Cu(I) Halide Complexes Showing TADF Combined with Room Temperature Phosphorescence: The Balance Tuned by Halogens. *Dalton Trans* 2020, 49, 3155–3163.
15. Zink DM; Bächle M; Baumann T; Nieger M; Kühn M; Wang C; Klopper W; Monkowius U; Hofbeck T; Yersin H, Synthesis, Structure, and Characterization of Dinuclear Copper(I) Halide Complexes with P^NN Ligands Featuring Exciting Photoluminescence Properties. *Inorg. Chem* 2013, 52, 2292–2305. [PubMed: 23061380]
16. Pearson RG, Hard and Soft Acids and Bases. *J. Am. Chem. Soc* 1963, 85, 3533–3539.
17. Shahsavari HR; Babadi Aghakhanpour R; Nikraves M; Ozdemir J; Golbon Haghghi M; Notash B; Beyzavi MH, Highly Emissive Cycloplatinated(II) Complexes Obtained by the Chloride Abstraction from the Complex [Pt(ppy)(PPh₃)(Cl)]: Employing Various Silver Salts. *Organometallics* 2018, 37, 2890–2900.
18. Fereidoonezhad M; Shahsavari HR; Abedanzadeh S; Behchenari B; Hossein-Abadi M; Faghhih Z; Beyzavi MH, Cycloplatinated(II) Complexes Bearing 1,1'-Bis(diphenylphosphino)ferrocene Ligand: Biological Evaluation and Molecular Docking Studies. *New J. Chem* 2018, 42, 2385–2392.
19. Fereidoonezhad M; Kaboudin B; Mirzaee T; Babadi Aghakhanpour R; Golbon Haghghi M; Faghhih Z; Faghhih Z; Ahmadipour Z; Notash B; Shahsavari HR, Cyclometalated Platinum(II) Complexes Bearing Bidentate O,O'-Di(alkyl)dithiophosphate Ligands: Photoluminescence and Cytotoxic Properties. *Organometallics* 2017, 36, 1707–1717.
20. Shahsavari HR; Giménez N; Lalinde E; Moreno MT; Fereidoonezhad M; Babadi Aghakhanpour R; Khatami M; Kalantari F; Jamshidi Z; Mohammadpour M, Heterobimetallic Pt^{II}-Au^I Complexes Comprising Unsymmetrical 1,1-Bis(diphenylphosphanyl)methane Bridges: Synthesis, Photophysical, and Cytotoxic Studies. *Eur. J. Inorg. Chem* 2019, 2019, 1360–1373.
21. Jamshidi M; Babaghasabha M; Shahsavari HR; Nabavizadeh SM, The Influence of Thiolate Ligands on the Luminescence Properties of Cycloplatinated(II) Complexes. *Dalton Trans* 2017, 46, 15919–15927. [PubMed: 29119183]

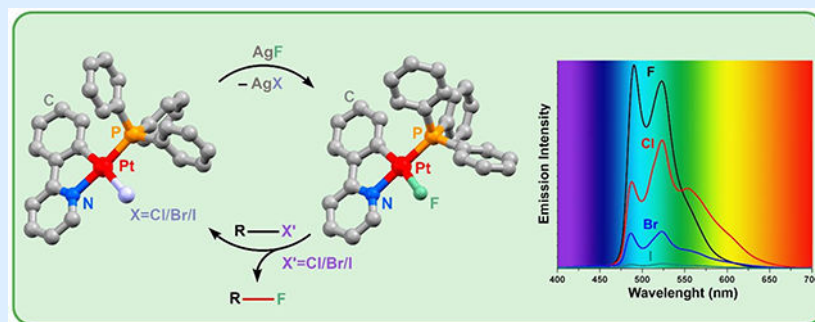
22. Nazari M; Shahsavari HR, Strong Red Emissions Induced by Pt–Pt Interactions in Binuclear Cycloplatinated(II) Complexes Containing Bridging Diphosphines. *Appl. Organomet. Chem* 2019, 33, e5020.
23. Joksch M; Agarwala H; Ferro M; Michalik D; Spannenberg A; Beweries T, A Comparative Study on the Thermodynamics of Halogen Bonding of Group 10 Pincer Fluoride Complexes. *Chem. Eur. J* 2019, 26, 3571–3577.
24. Nova A; Erhardt S; Jasim NA; Perutz RN; Macgregor SA; McGrady JE; Whitwood AC, Competing C–F Activation Pathways in the Reaction of Pt(0) with Fluoropyridines: Phosphine-Assistance versus Oxidative Addition. *J. Am. Chem. Soc* 2008, 130, 15499–15511. [PubMed: 18950168]
25. Yahav A; Goldberg I; Vigalok A, Difluoro Complexes of Platinum(II) and-(IV) with Monodentate Phosphine Ligands: An Exceptional Stability of d^6 Octahedral Organometallic Fluorides. *Inorg. Chem* 2005, 44, 1547–1553. [PubMed: 15732997]
26. Zhao S-B; Wang R-Y; Nguyen H; Becker JJ; Gagné MR, Electrophilic Fluorination of Cationic Pt-Aryl Complexes. *Chem. Commun* 2012, 48, 443–445.
27. Nilsson P; Plamper F; Wendt OF, Synthesis, Structure, and Reactivity of Arylfluoro Platinum(II) Complexes. *Organometallics* 2003, 22, 5235–5242.
28. Berger J; Braun T; Ahrens T; Klaering P; Laubenstein R; Braun-Cula B, The Versatile Behavior of Platinum Alkyne Complexes towards XeF^2 : Formation of Fluorovinyl and Fluorido Complexes. *Chem. Eur. J* 2017, 23, 8886–8900. [PubMed: 28472555]
29. Anderson CM; Crespo M; Ferguson G; Lough AJ; Puddephatt RJ, Activation of Aromatic Carbon-Fluorine Bonds by Organoplatinum Complexes. *Organometallics* 1992, 11, 1177–1181.
30. López O; Crespo M; Font-Bardía M; Solans X, Activation of C–F and C–H Bonds by Platinum in Trifluorinated [C,N,N'] Ligands. Crystal Structures of [PtFMe₂{Me₂NCH₂CH₂NHCH(CH₂COMe)(2,4-C₆H₂F₂)}] and [PtMe{Me₂NCH₂CH₂NCH(2,3,4-C₆HF₃)}]. *Organometallics* 1997, 16, 1233–1240.
31. Abo-Amer A; Boyle PD; Puddephatt RJ, Oxidation of a Dimethyl Platinum(II) Complex with Xenon Difluoride: The Important Role of Solvent. *Inorg. Chem. Commun* 2015, 61, 193–196.
32. Anderson CM; Puddephatt RJ; Ferguson G; Lough AJ, Oxidative Addition of Aryl–Halogen Bonds to Platinum(II) and the Structure of a Complex Formed by Aryl–Fluoride Oxidative Addition. *J. Chem. Soc., Chem. Commun* 1989, 1297–1298.
33. Berger J; Braun T; Herrmann R; Braun B, Reactivity of Platinum Alkyne Complexes Towards N-Fluorobenzenesulfonimide: Formation of Platinum Compounds Bearing a β -Fluorovinyl Ligand. *Dalton Trans* 2015, 44, 19553–19565. [PubMed: 26308149]
34. Kaspi AW; Goldberg I; Vigalok A, Reagent-Dependent Formation of C–C and C–F Bonds in Pt Complexes: An Unexpected Twist in the Electrophilic Fluorination Chemistry. *J. Am. Chem. Soc* 2010, 132, 10626–10627. [PubMed: 20681679]
35. Dubinsky-Davidchik I; Goldberg I; Vigalok A; Vedernikov AN, Selective Aryl–Fluoride Reductive Elimination from a Platinum(IV) Complex. *Angew. Chem. Int. Ed* 2015, 54, 12447–12451.
36. Yahav-Levi A; Goldberg I; Vigalok A, Synthesis and Reactivity of Unsymmetrical Difluoro Pt(IV) Complexes. *J. Fluor. Chem* 2010, 131, 1100–1102.
37. Dubinsky-Davidchik IS; Goldberg I; Vigalok A; Vedernikov AN, Unprecedented 1,3-Migration of the Aryl Ligand in Metallacyclic Aryl α -Naphthyl Pt(IV) Difluorides to Produce β -Arylnaphthyl Pt(II) Complexes. *Chem. Commun* 2013, 49, 3446–3448.
38. Vigalok A, Electrophilic Halogenation–Reductive Elimination Chemistry of Organopalladium and -Platinum Complexes. *Acc. Chem. Res* 2015, 48, 238–247. [PubMed: 25602260]
39. Crespo M, Fluorine in Cyclometalated Platinum Compounds. *Organometallics* 2012, 31, 1216–1234.
40. Crespo M; Martínez M; Nabavizadeh SM; Rashidi M, Kinetic-Mechanistic Studies on C–X (X = H, F, Cl, Br, I) Bond Activation Reactions on Organoplatinum(II) Complexes. *Coord. Chem. Rev* 2014, 279, 115–140.
41. Niazi M; Shahsavari HR; Golbon Haghghi M; Halvagar MR; Hatami S; Notash B, Reactivity of a Half-Lantern Pt₂(II,II) Complex with Triphenylphosphine: Selectivity in Protonation Reaction. *RSC Adv* 2016, 6, 76463–76472.

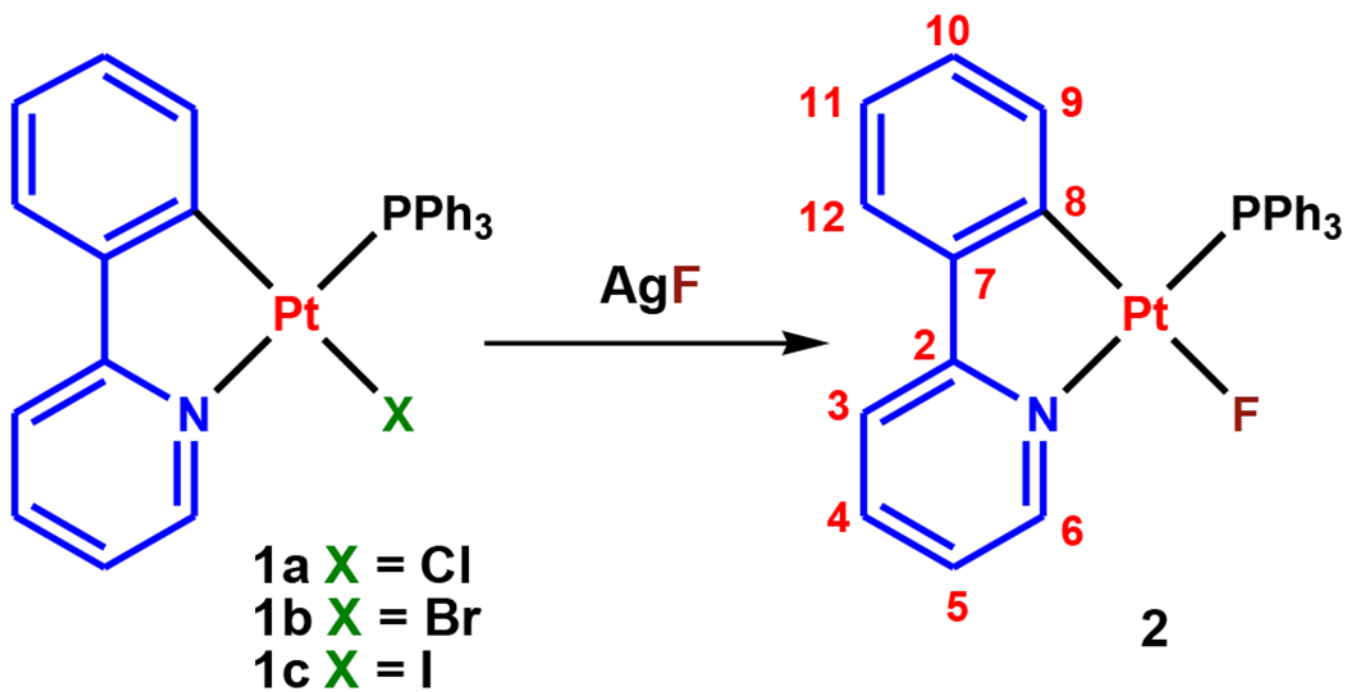
42. Niazi M; Shahsavari HR; Golbon Haghighi M; Halvagar MR; Hatami S; Notash B, Carbon-Sulfur Bond Reductive Coupling from a Platinum(II) Thiolate Complex. *RSC Adv* 2016, 6, 95073–95084.
43. Allen FH; Wood PA; Galek PTA, Role of Chloroform and Dichloromethane Solvent Molecules in Crystal Packing: An Interaction Propensity Study. *Acta Cryst.* 2013, B69, 379–388.
44. Dalvit C; Vulpetti A, Weak Intermolecular Hydrogen Bonds with Fluorine: Detection and Implications for Enzymatic/Chemical Reactions, Chemical Properties, and Ligand/Protein Fluorine NMR Screening. *Chem. Eur. J* 2016, 22, 7592–7601. [PubMed: 27112430]
45. Champagne PA; Desroches J; Paquin J-F, Organic Fluorine as a Hydrogen-Bond Acceptor: Recent Examples and Applications. *Synthesis* 2015, 47, 306–322.
46. Schneider H-J, Hydrogen Bonds with Fluorine. Studies in Solution, in Gas Phase and by Computations, Conflicting Conclusions from Crystallographic Analyses. *Chemical Science* 2012, 3, 1381–1394.
47. Shahsavari HR; Babadi Aghakhanpour R; Biglari A; Niazi M; Mastrorilli P; Todisco S; Gallo V; Lalinde E; Moreno MT; Giménez N; Halvagar MR, C(sp²)-C(sp²) Reductive Elimination from a Diarylplatinum(II) Complex Induced by a S–S Bond Oxidative Addition at Room Temperature. *Organometallics* 2020, 39, 417–424.
48. Lin X; Weng Z, Transition Metal Complex Assisted C_{sp3}-F Bond Formation. *Dalton Trans* 2015, 44, 2021–2037. [PubMed: 25515695]
49. Campbell MG; Hoover AJ; Ritter T, Transition Metal-Mediated and Metal-Catalyzed Carbon–Fluorine Bond Formation In Organometallic Fluorine Chemistry, Braun T; Hughes RP, Eds. Springer International Publishing: Cham, 2015; pp 1–53.
50. Hu J-Y; Zhang J-L, Hydrodefluorination Reactions Catalyzed by Transition-Metal Complexes. *Top. Organomet. Chem* 2015, 52, 143–196.
51. Kuehnle MF; Lentz D; Braun T, Synthesis of Fluorinated Building Blocks by Transition-Metal-Mediated Hydrodefluorination Reactions. *Angew. Chem. Int. Ed* 2013, 52, 3328–3348.
52. Ahrens T; Kohlmann J; Ahrens M; Braun T, Functionalization of Fluorinated Molecules by Transition-Metal-Mediated C–F Bond Activation to Access Fluorinated Building Blocks. *Chem. Rev* 2015, 115, 931–972. [PubMed: 25347593]
53. Hintermann L; Läng F; Maire P; Togni A, Interactions of Cationic Palladium(II)- and Platinum(II)- η^3 -Allyl Complexes with Fluoride: Is Asymmetric Allylic Fluorination a Viable Reaction? *Eur. J. Inorg. Chem* 2006, 2006, 1397–1412.
54. Armarego WLF, Purification of Laboratory Chemicals. 8th ed.; Butterworth-Heinemann 2017.
55. Bruker SAINT, Version 6.36 a. Bruker-AXS Inc.: Madison, WI, USA 2002.
56. Bruker SMART, Version 5.625 and SADABS, Version 2.03 a. Bruker AXS Inc., Madison, Wisconsin 2001.
57. Sheldrick GM, A Short History of *SHELX*. *Acta Cryst.* 2008, A64, 112–122.
58. Sheldrick GM, Crystal Structure Refinement with *SHELXL*. *Acta Cryst.* 2015, C27, 3–8.
59. Frisch MJ; Trucks GW; Schlegel HB; Scuseria GE; Robb MA; Cheeseman JR; Scalmani G; Barone V; Mennucci B; Petersson GA; Nakatsuji H; Caricato M; Li X; Hratchian HP; Izmaylov AF; Bloino J; Zheng G; Sonnenberg JL; Hada M; Ehara M; Toyota K; Fukuda R; Hasegawa J; Ishida M; Nakajima T; Honda Y; Kitao O; Nakai H; Vreven T; Montgomery JJA; Peralta JE; Ogliaro F; Bearpark M; Heyd JJ; Brothers E; Kudin KN; Staroverov VN; Keith T; Kobayashi R; Normand J; Raghavachari K; Rendell A; Burant JC; Iyengar SS; Tomasi J; Cossi M; Rega N; Millam JM; Klene M; Knox JE; Cross JB; Bakken V; Adamo C; Jaramillo J; Gomperts R; Stratmann RE; Yazyev O; Austin AJ; Cammi R; Pomelli C; Ochterski JW; Martin RL; Morokuma K; Zakrzewski VG; Voth GA; Salvador P; Dannenberg JJ; Dapprich S; Daniels AD; Farkas O; Foresman JB; Ortiz JV; Cioslowski J; Fox DJ, Gaussian 09, Revision A.02. 2016; p Gaussian, Inc., Wallingford CT.
60. Becke AD, Density-functional Thermochemistry. III. The Role of Exact Exchange. *J. Chem. Phys* 1993, 98, 5648–5652.
61. Miehlich B; Savin A; Stoll H; Preuss H, Results Obtained with the Correlation Energy Density Functionals of Becke and Lee, Yang and Parr. *Chem. Phys. Lett* 1989, 157, 200–206.

62. Lee C; Yang W; Parr RG, Development of the Colle-Salvetti Correlation-Energy Formula into a Functional of the Electron Density. *Phys. Rev. B* 1988, 37, 785.
63. Wadt WR; Hay PJ, Ab Initio Effective Core Potentials for Molecular Calculations. Potentials for Main Group Elements Na to Bi. *J. Chem. Phys* 1985, 82, 284–298.
64. Roy LE; Hay PJ; Martin RL, Revised Basis Sets for the LANL Effective Core Potentials. *J. Chem. Theory Comput* 2008, 4, 1029–1031. [PubMed: 26636355]
65. Cossi M; Scalmani G; Rega N; Barone V, New Developments in the Polarizable Continuum Model for Quantum Mechanical and Classical Calculations on Molecules in Solution. *J. Chem. Phys* 2002, 117, 43–54.
66. Barone V; Cossi M; Tomasi J, A New Definition of Cavities for the Computation of Solvation Free Energies by the Polarizable Continuum Model. *J. Chem. Phys* 1997, 107, 3210–3221.

SYNOPSIS

A cycloplatinated(II) fluoride complex was prepared and it revealed an interesting photophysical properties and reactivity for Csp^3-F bond formation.





Scheme 1.
Synthetic route and ligand numbering system for 2.

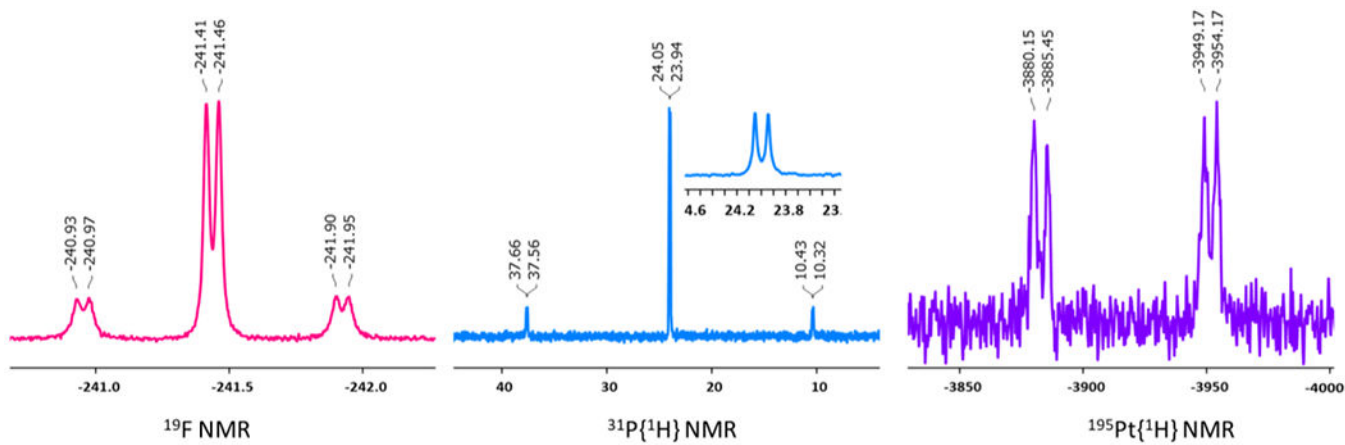


Figure 1.
Heteronuclear NMR spectra of **2** in CD_2Cl_2 .

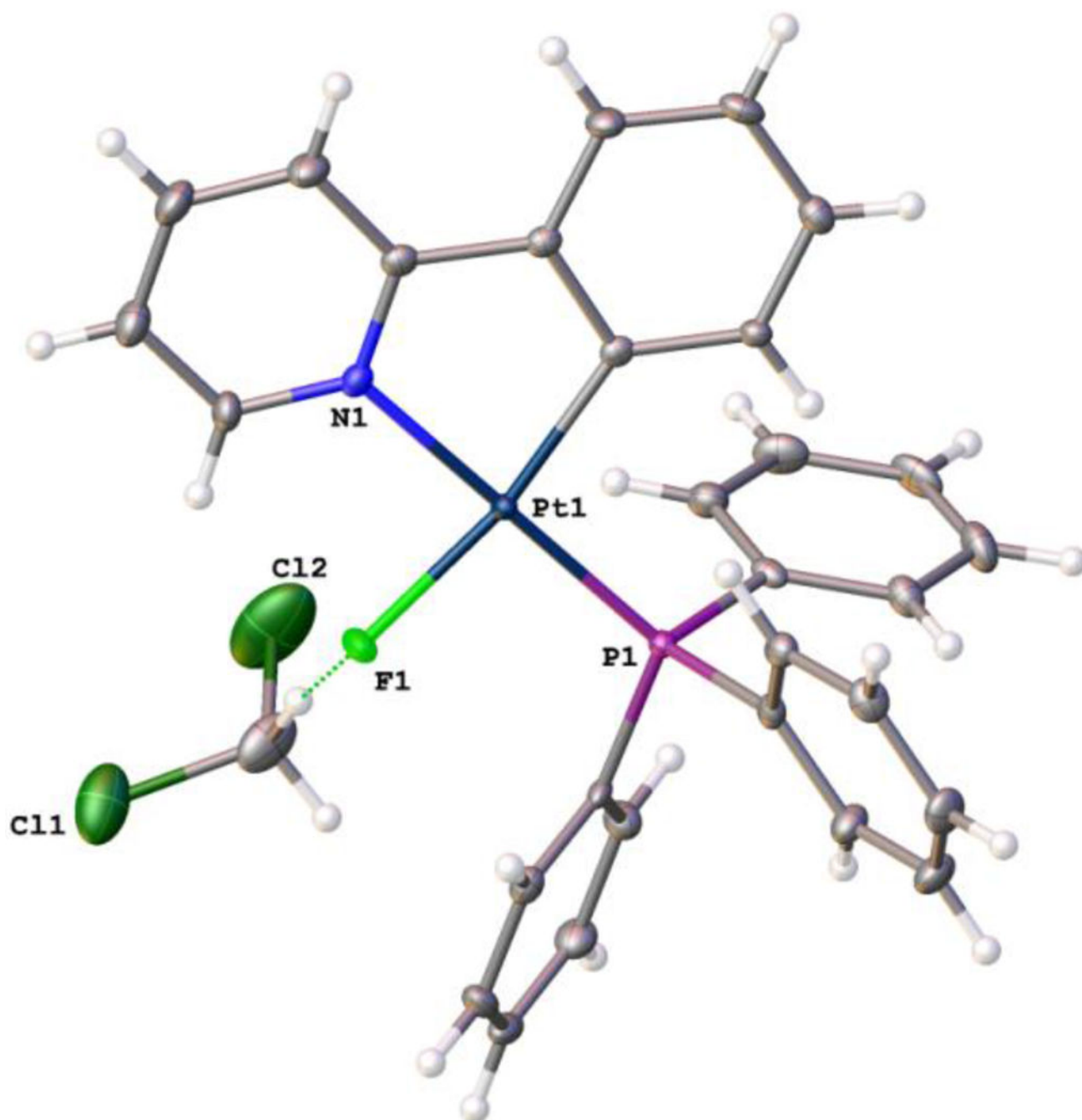


Figure 2.

Molecular structure of **2**·CH₂Cl₂. Ellipsoids are drawn at a 50% probability level. Selected bond lengths (Å) and angles (deg): Pt(1)-P(1) 2.2288(7), Pt(1)-F(1) 2.0417(18), Pt(1)-N(1) 2.057(2), Pt(1)-C(11) 1.994(3); F(1)-Pt(1)-P(1) 91.87(5), F(1)-Pt(1)-N(1) 87.88(9), C(11)-Pt(1)-P(1) 98.88(8), C(11)-Pt(1)-N(1) 81.38(11).

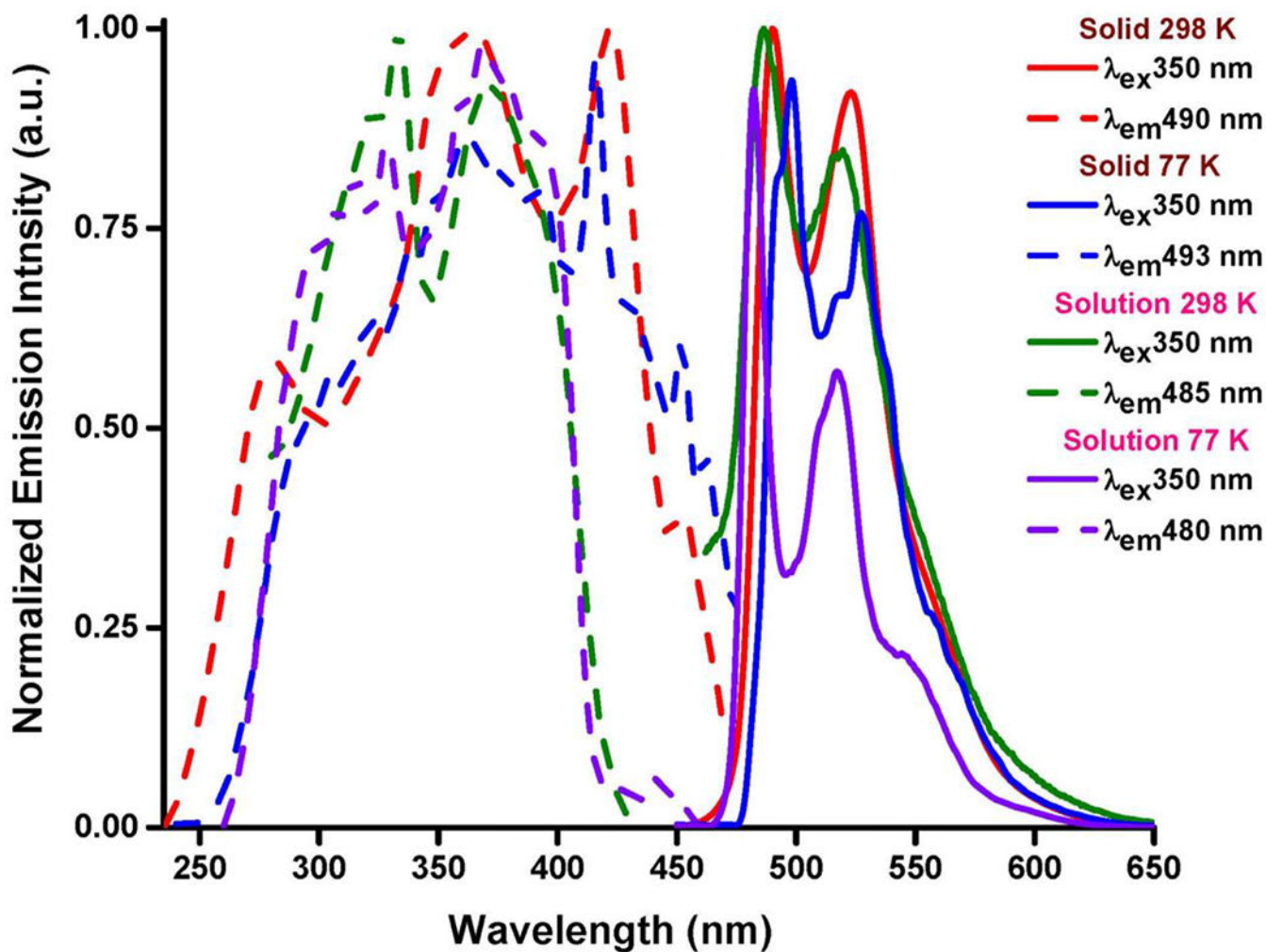


Figure 3. Normalized emission (solid lines) and excitation (dashed lines) spectra of **2** in the solid state and CH_2Cl_2 solution (10^{-3} M) at 298 and 77 K.

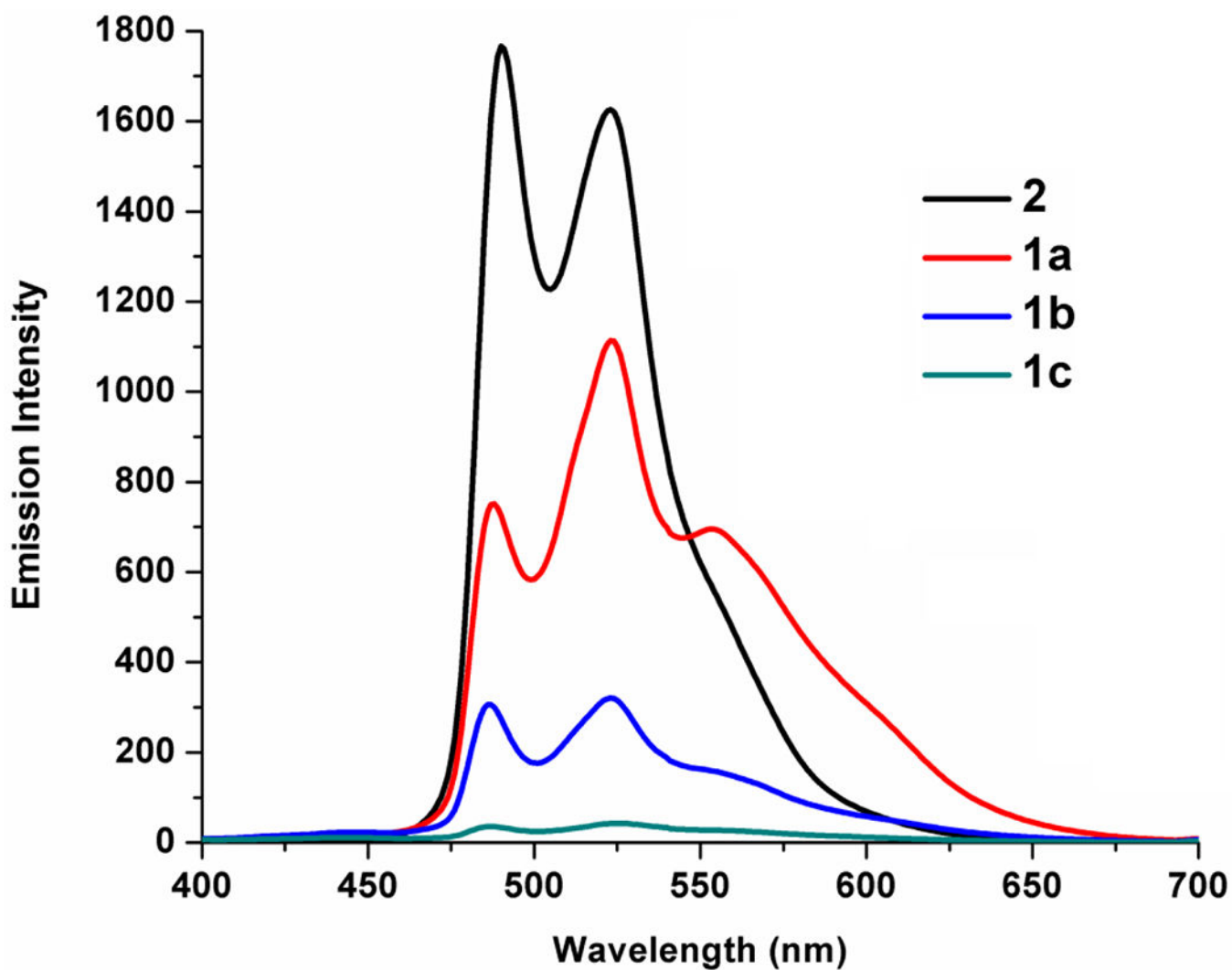


Figure 4.
The emission spectra of **1a**–**c** and **2** in solid state at 298 K ($\lambda_{\text{ex}} = 350$ nm).

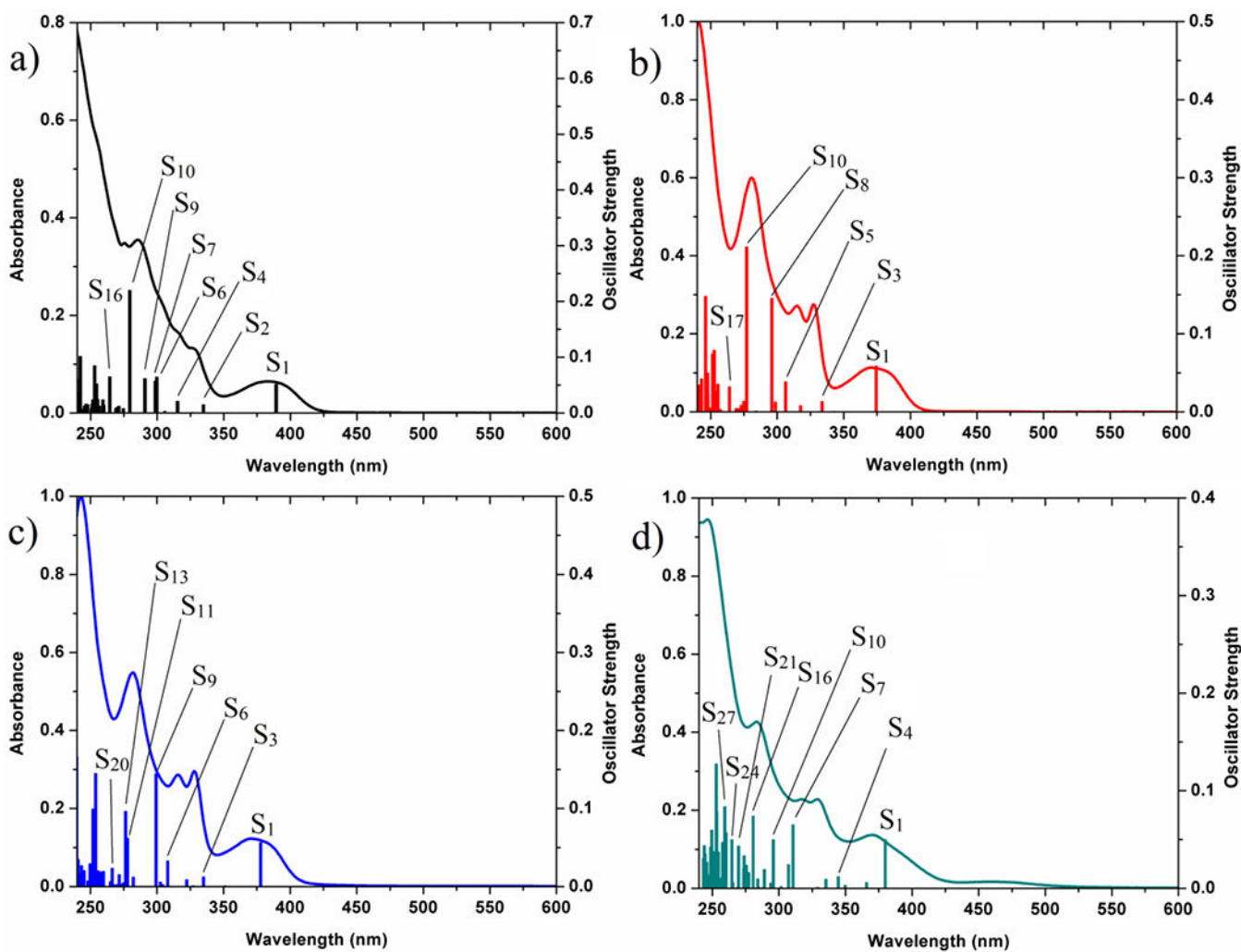


Figure 5.
Overlaid experimental UV-vis spectra and theoretical TD-DFT bars for (a) **2**, (b) **1a**, (c) **1b**
and (d) **1c**.

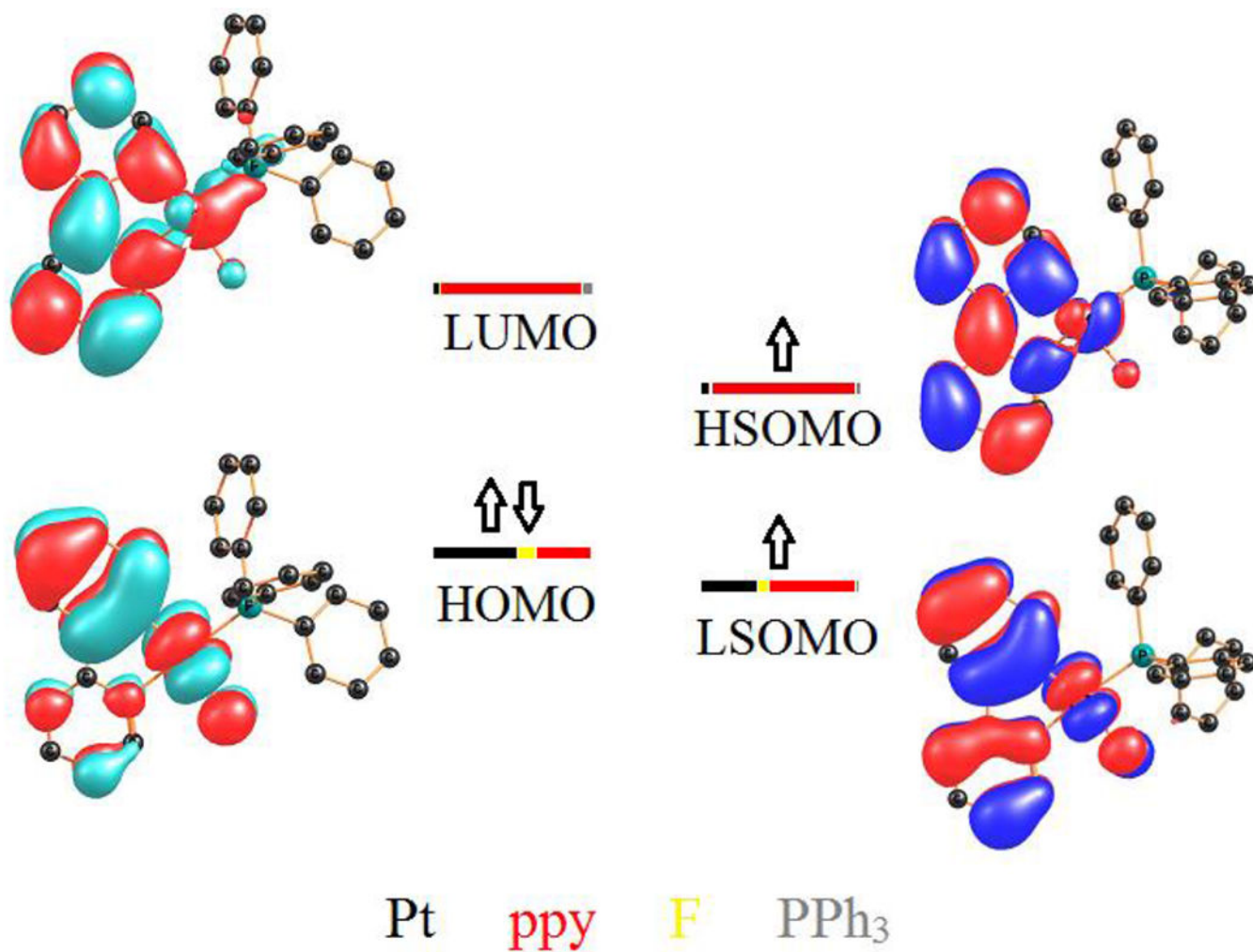


Figure 6. Frontier molecular orbital plots of the calculated S₀ (left) and T₁ (right) states of **2**.

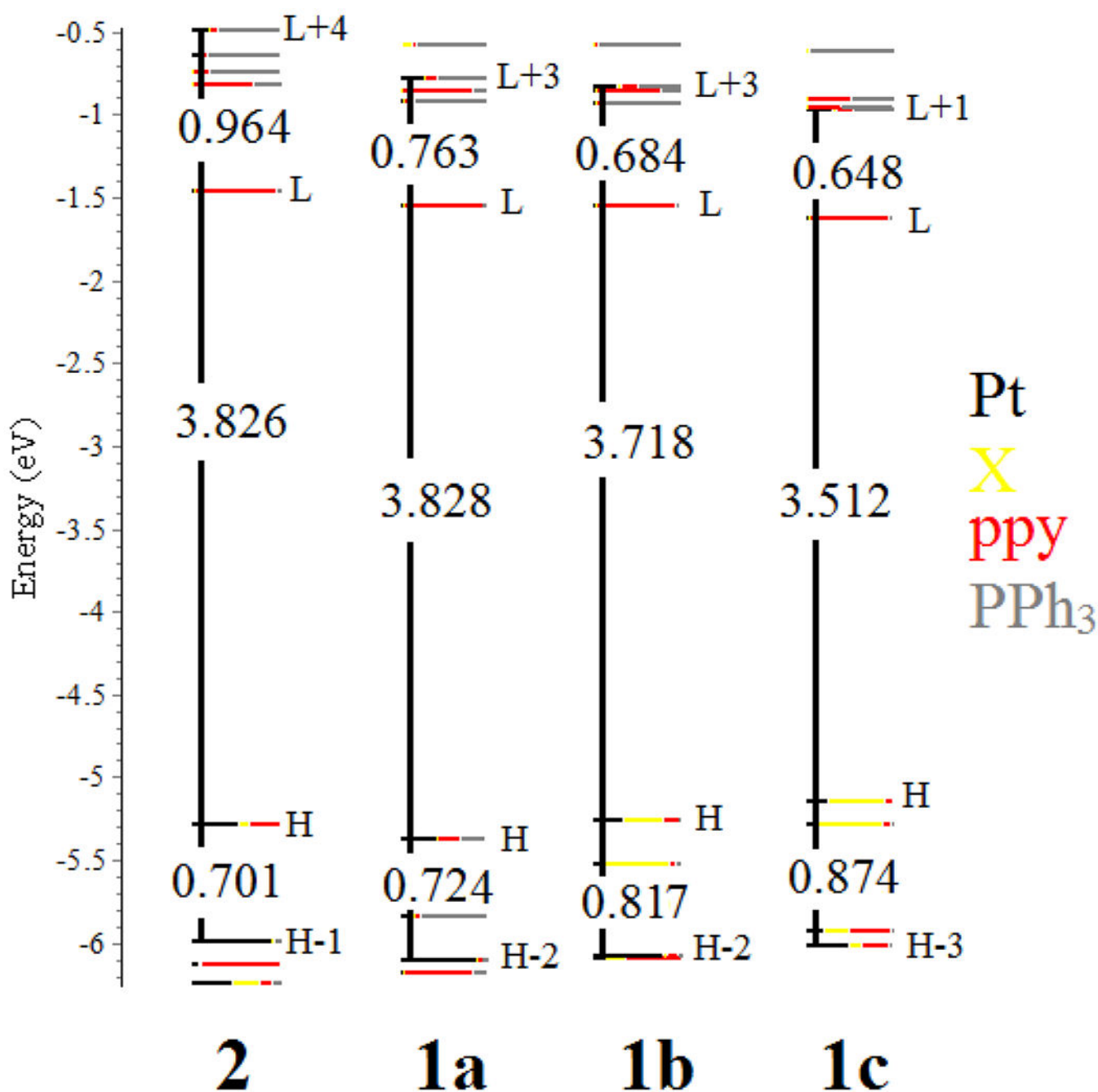


Figure 7. Comparative energy level diagram for the calculated MOs of **1a-c** and **2** in the gas phase. The energy values are shown in eV.

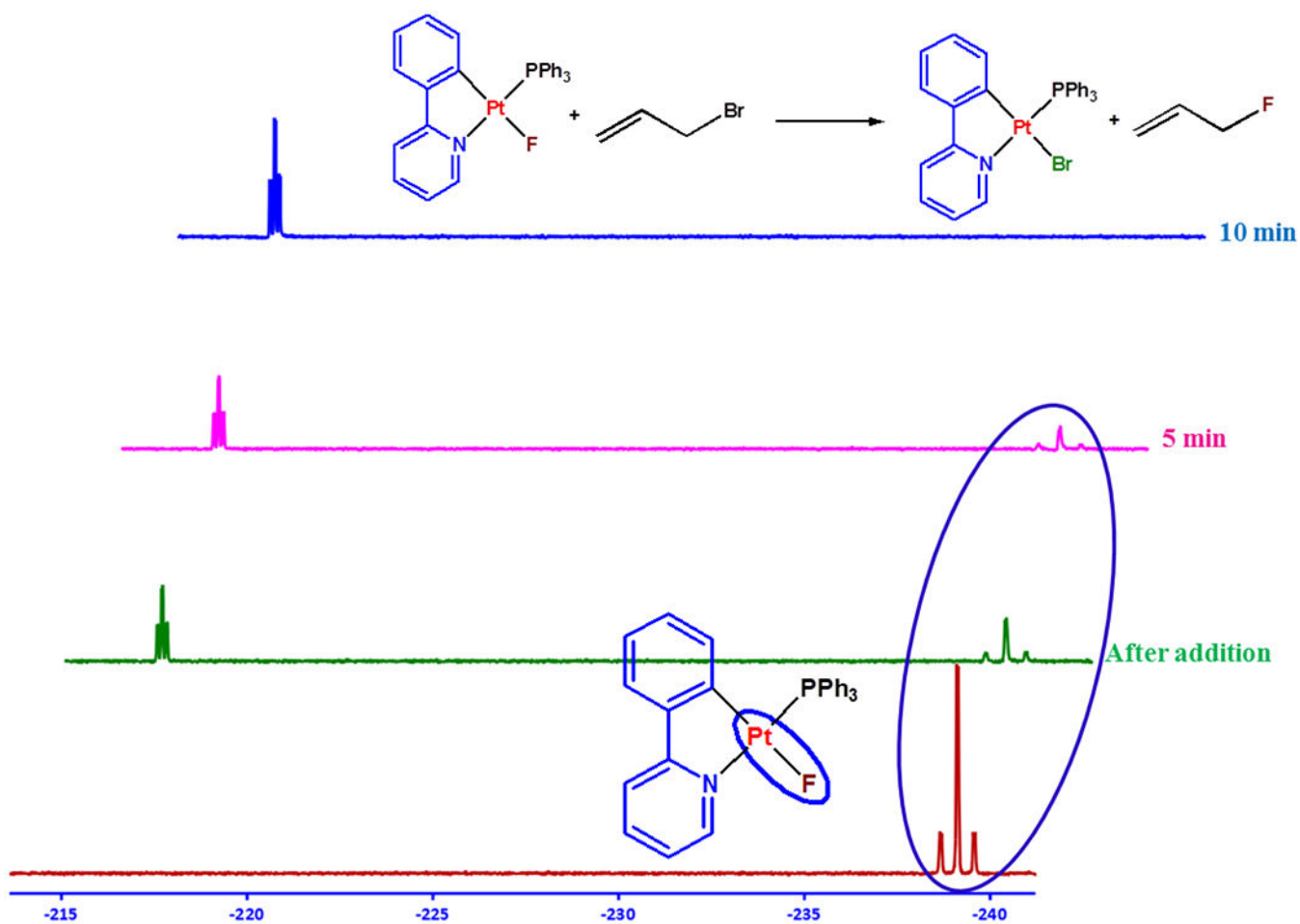


Figure 8. Monitoring the reaction of **2** with allyl bromide by ^{19}F NMR spectroscopy in acetone- d_6 at room temperature.

Table 1.Numerical data of the emission properties of **1a**, **1b** and **2**.

| Complex | λ_{em}/nm (λ_{ex}/nm) | $\tau/\mu s$ | $\Phi(\%)$ | k_r^a | k_{nr}^a |
|-----------|--|--------------|------------|--------------------|--------------------|
| 2 | 490 ^{max} , 522, 560 ^{sh} | 11.6 | 53.1 | 4.56×10^4 | 4.06×10^4 |
| | (350), Solid (298 K) | 21.5 | 94.6 | 4.40×10^4 | 0.25×10^4 |
| | 493 ^{max} , 529, 560 ^{sh} | 2.3 | 8.4 | 3.65×10^4 | 39.8×10^4 |
| | (350), Solid (77 K) | 16.5 | 88.1 | 4.67×10^4 | 1.39×10^4 |
| | 485 ^{max} , 518, 555 ^{sh} | | | | |
| | (350), 10^{-3} M (298 K) | | | | |
| 1a | 480 ^{max} , 516, | | | | |
| | 551 ^{sh} (350), 10^{-3} M (77 K) | | | | |
| 1a | 487, 522 ^{max} , 554 ^{sh} (350), Solid (298 K) | 7.2 | 47.0 | 6.52×10^4 | 7.36×10^4 |
| 1b | 487, 522 ^{max} , 554 ^{sh} (350), Solid (298 K) | 6.9 | 31.0 | 4.49×10^4 | 10.0×10^4 |

^a k_r and k_{nr} were calculated according to the equations $k_r = \Phi/\tau$ and $k_{nr} = (1/\tau) - k_r$ respectively.

Table 2.Composition (%) of the selected MOs in S_0 and T_1 states in gas phase for **2** (X = F) and **1a-c** (X = Cl, Br, I).

| Complex | MO | Energy (eV) | Components (%) | | | |
|-----------|--------|-------------|----------------|----|-----|------------------|
| | | | Pt | X | ppy | PPh ₃ |
| 2 | LUMO+4 | -0.495 | 20 | 1 | 9 | 69 |
| | LUMO | -1.459 | 5 | 1 | 88 | 7 |
| | HOMO | -5.285 | 52 | 11 | 35 | 1 |
| | HOMO-1 | -5.986 | 89 | 1 | 2 | 8 |
| | HSOMO | -2.926 | 6 | 1 | 90 | 3 |
| | LSOMO | -5.768 | 36 | 7 | 54 | 2 |
| 1a | LUMO+3 | -0.784 | 28 | 0 | 14 | 58 |
| | LUMO | -1.547 | 5 | 1 | 89 | 6 |
| | HOMO | -5.375 | 43 | 30 | 27 | 1 |
| | HOMO-2 | -6.099 | 85 | 0 | 6 | 9 |
| | HSOMO | -3.080 | 6 | 1 | 91 | 3 |
| | LSOMO | -5.809 | 34 | 29 | 35 | 1 |
| 1b | LUMO+3 | -0.862 | 28 | 4 | 19 | 49 |
| | LUMO | -1.546 | 5 | 1 | 89 | 5 |
| | HOMO | -5.264 | 35 | 45 | 18 | 1 |
| | HOMO-2 | -6.081 | 78 | 4 | 11 | 7 |
| | HSOMO | -3.015 | 7 | 1 | 87 | 4 |
| | LSOMO | -5.699 | 30 | 37 | 30 | 3 |
| 1c | LUMO+1 | -0.976 | 31 | 5 | 18 | 46 |
| | LUMO | -1.624 | 5 | 1 | 89 | 5 |
| | HOMO | -5.136 | 25 | 62 | 10 | 3 |
| | HOMO-3 | -6.010 | 49 | 15 | 31 | 5 |